Supporting Information

MgO Nanocubes as a Self-calibrating Optical Probes for Efficient Ratiometric Detection of the Picric Acid in Solid State

Subrata Senapati, Karuna Kar Nanda*

Materials Research Centre, Indian Institute of Science, Bangalore-560012, India.

*E-mail: nanda@iisc.ac.in

Number of pages: 23, Number of Figures: 19, Number of Tables: 4.

Content:

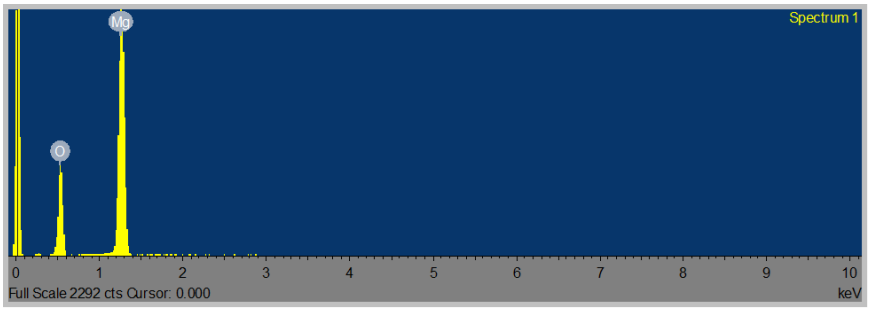

Figure S1. EDS spectrum of the MgO-600 nanocubes.

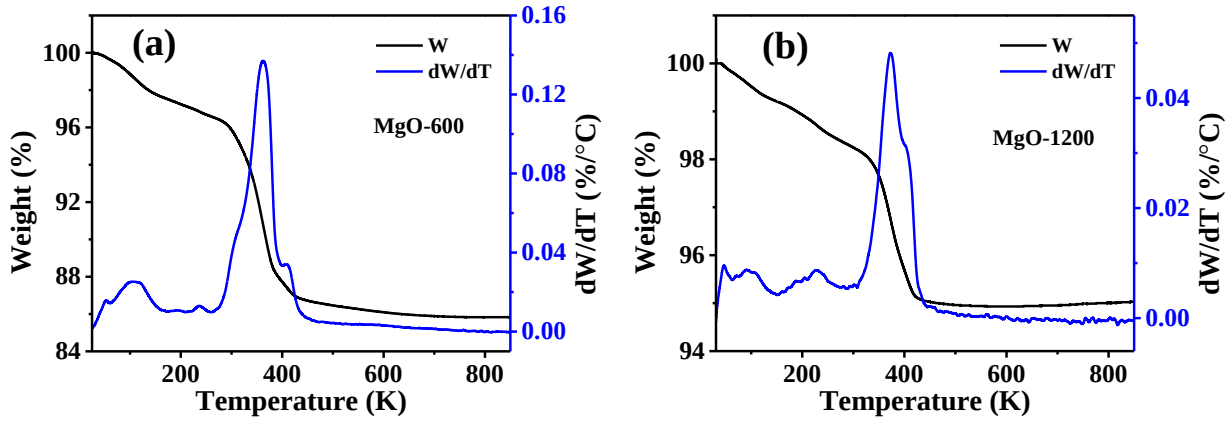

Figure S2. TGA curves of (a) MgO-600 and (b) MgO-1200, respectively.

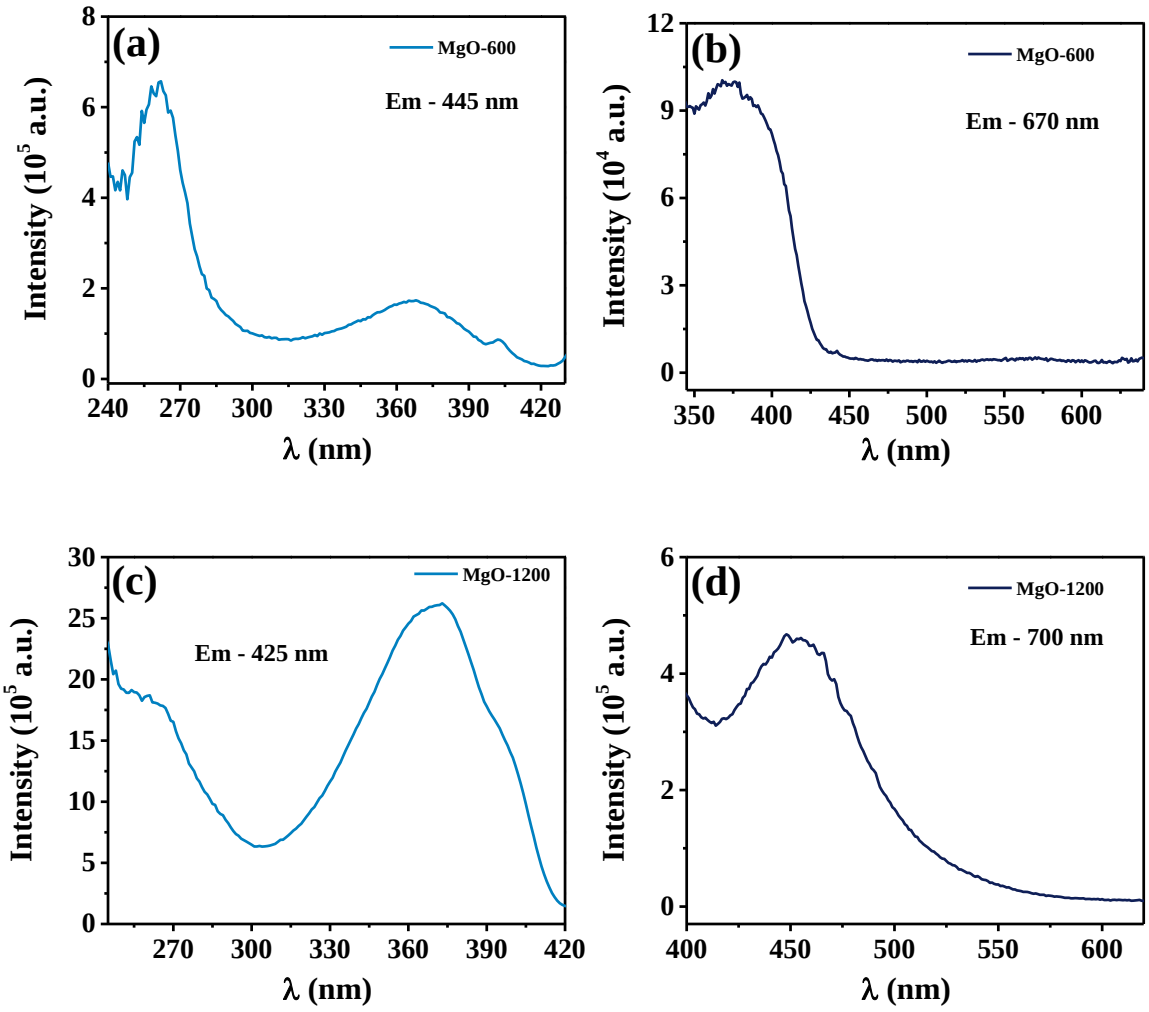

Figure S3. PL excitation spectra of (a, b) MgO-600 and (c, d) MgO-1200 for emission at (a) 445, (b) 670, (c) 425, and (d) 700 nm, respectively.

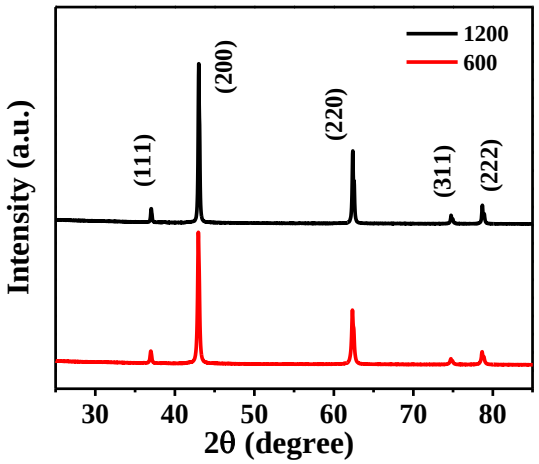

Figure S4. XRD patterns of the MgO-600 (O) and MgO-1200 (O).

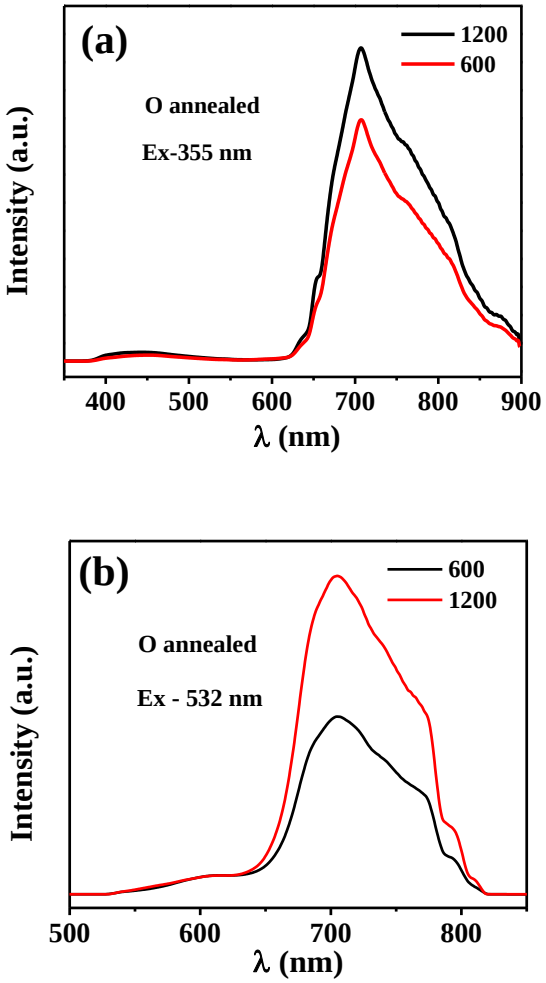

Figure S5. Room temperature PL spectra of the MgO-600 (O) and MgO-1200 (O) with (a) 355 nm and (b) 532 nm excitation, respectively.

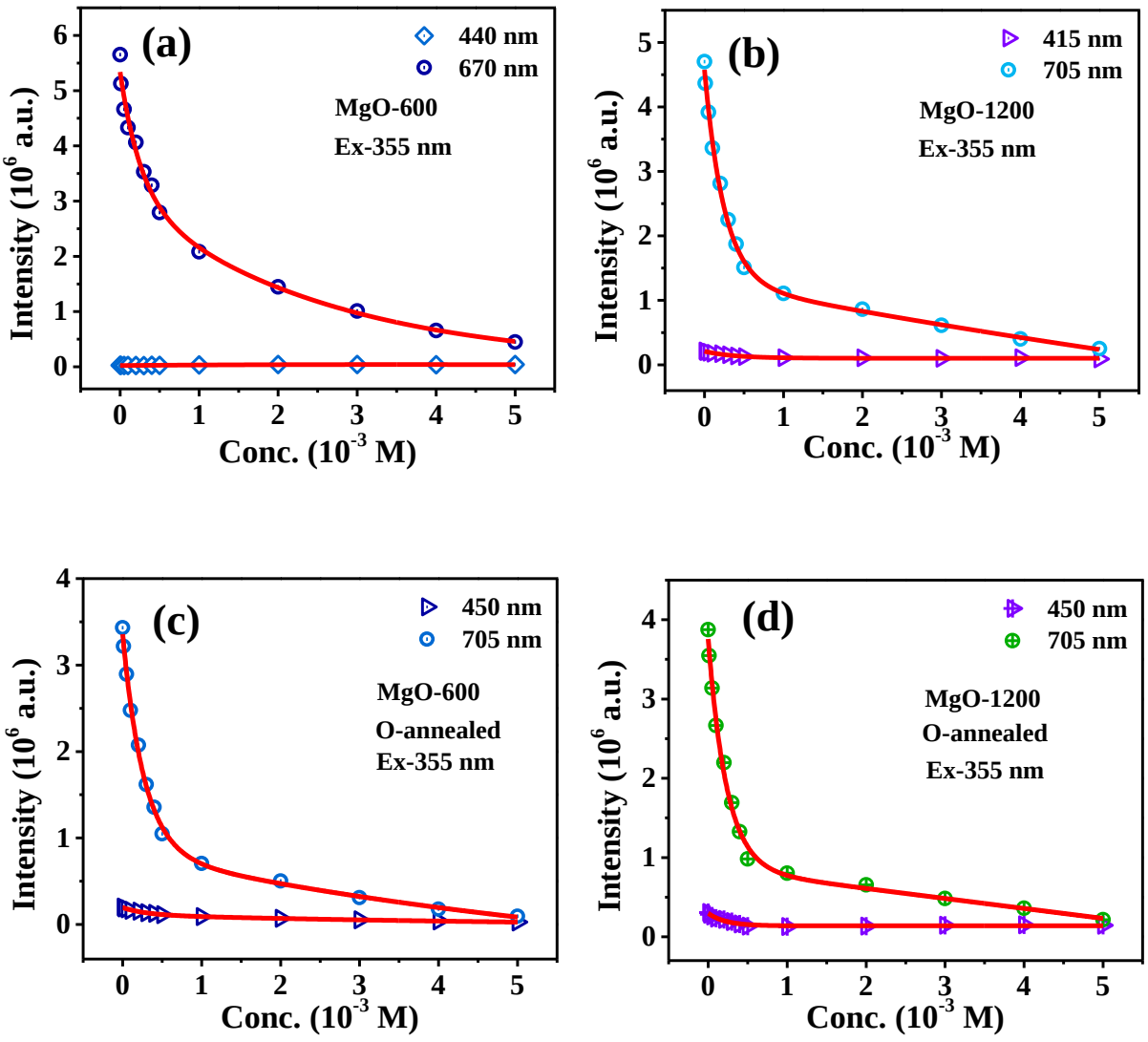

Figure S6. Variation of different integral peak intensities with increasing PA concentration of (a) MgO-600, (b) MgO-1200, (c) MgO-600 (O) and (d) MgO-1200 (O), respectively with 355 nm excitation.

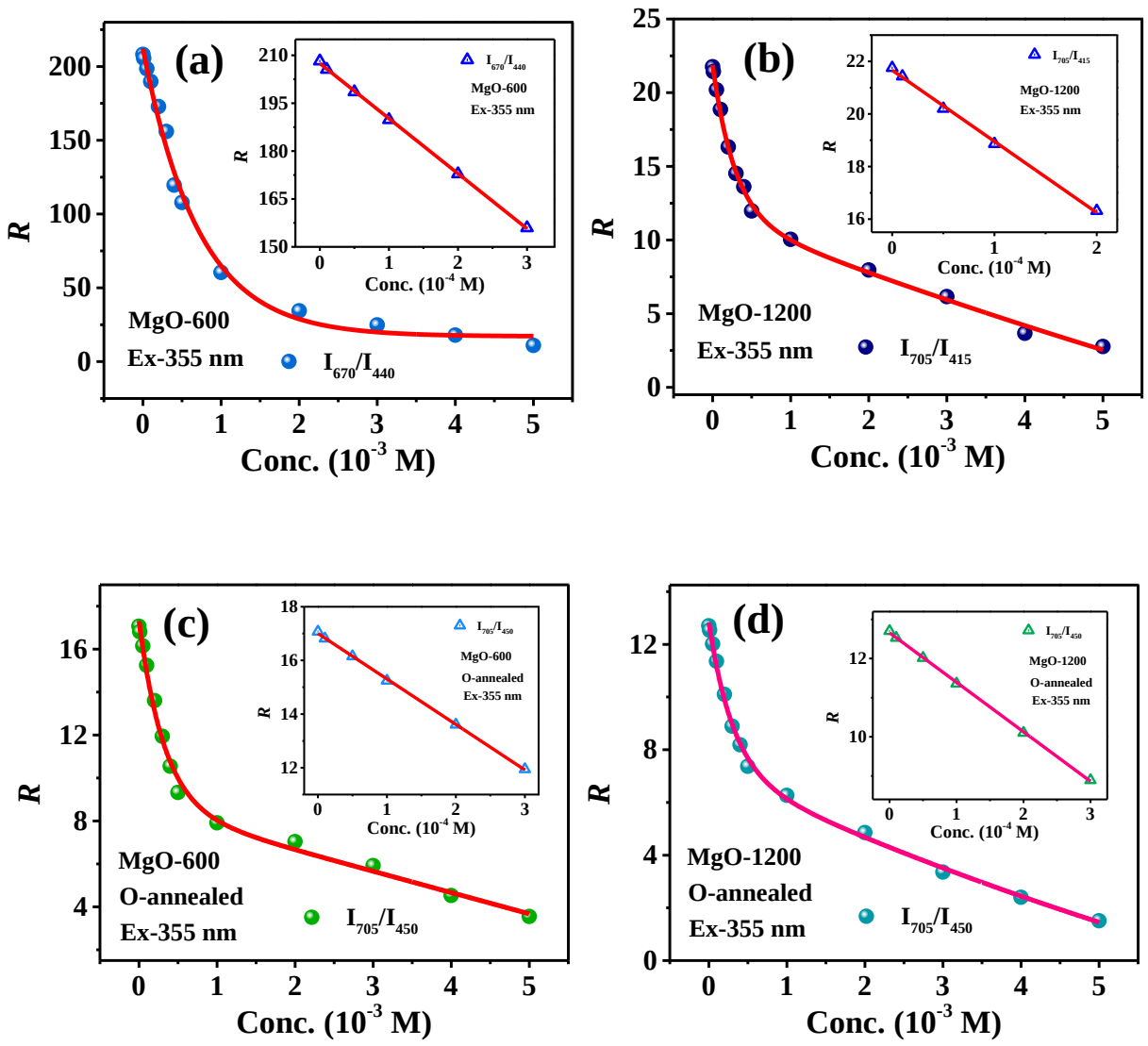

Figure S7. Variation of integral peak intensity ratio (R) with increasing PA concentration of (a) MgO-600, (b) MgO-1200, (c) MgO-600 (O) and (d) MgO-1200 (O), respectively with 355 nm excitation. Insets show the linear fitting of the plot in the low PA concentration region.

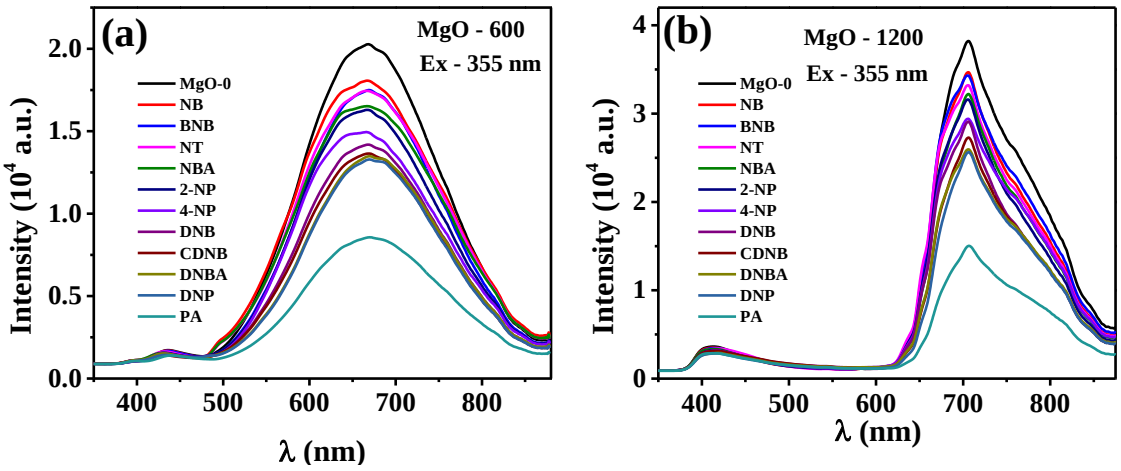

Figure S8. PL spectra in the presence of various nitro compounds (500 μM) for (a) MgO-600 and (b) MgO-1200 with 355 nm excitation.

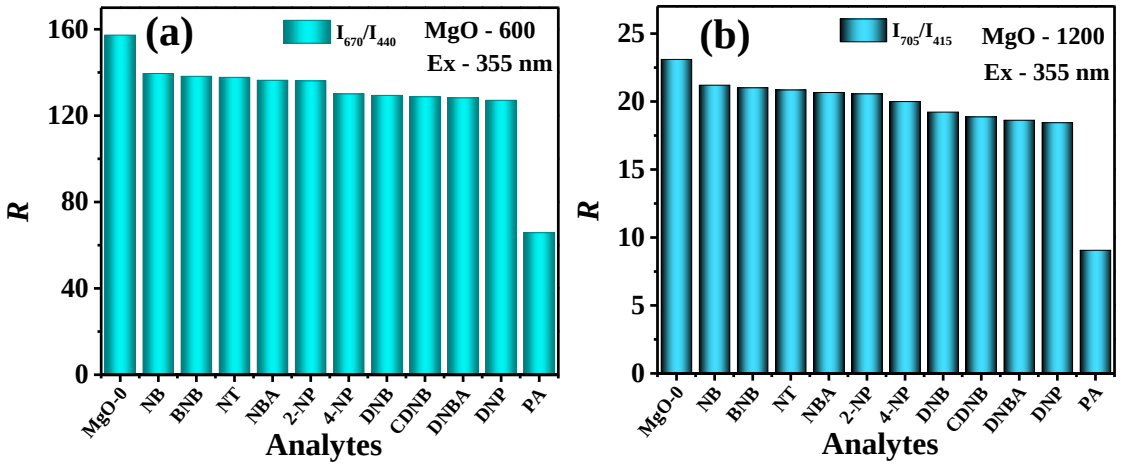

Figure S9. Variation of integral PL intensity ratio for different nitro compounds (500 μM) of (a) MgO-600 and (b) MgO-1200.

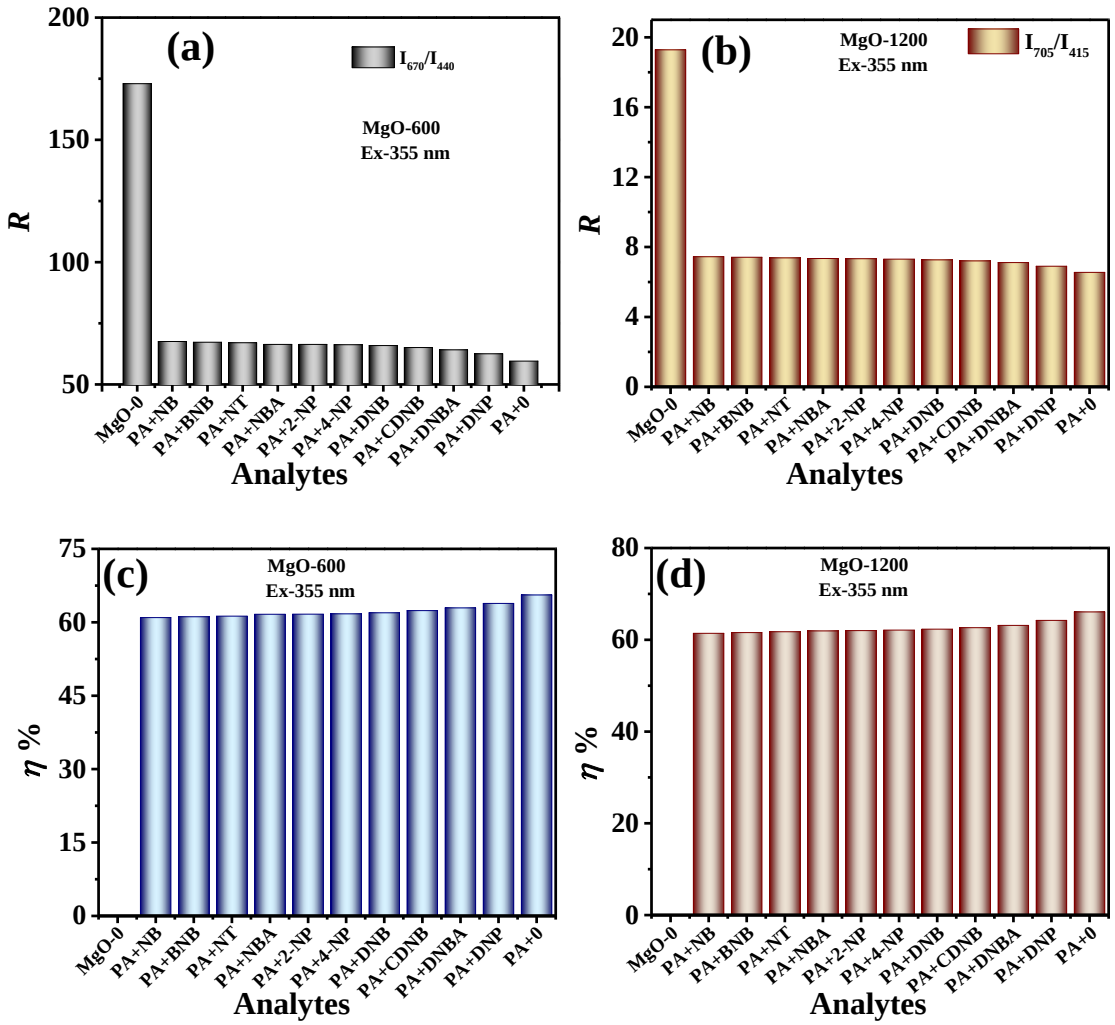

Figure S10. (a, b) Variation of integral PL intensity ratio for different nitro compounds (500 μM) in the presence of PA and (c, d) corresponding quenching efficiency for MgO-600 and MgO-1200, respectively.

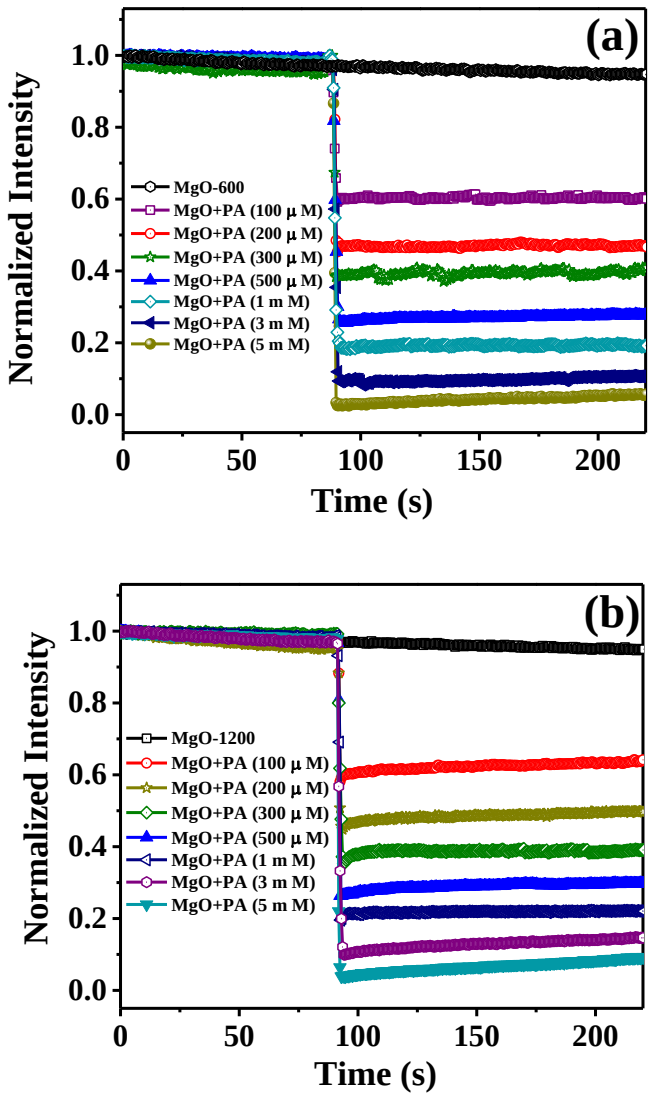

Figure S11. Temporal response curve for addition of different concentration of PA on MgO film for (a) MgO-600 and (b) MgO-1200, respectively.

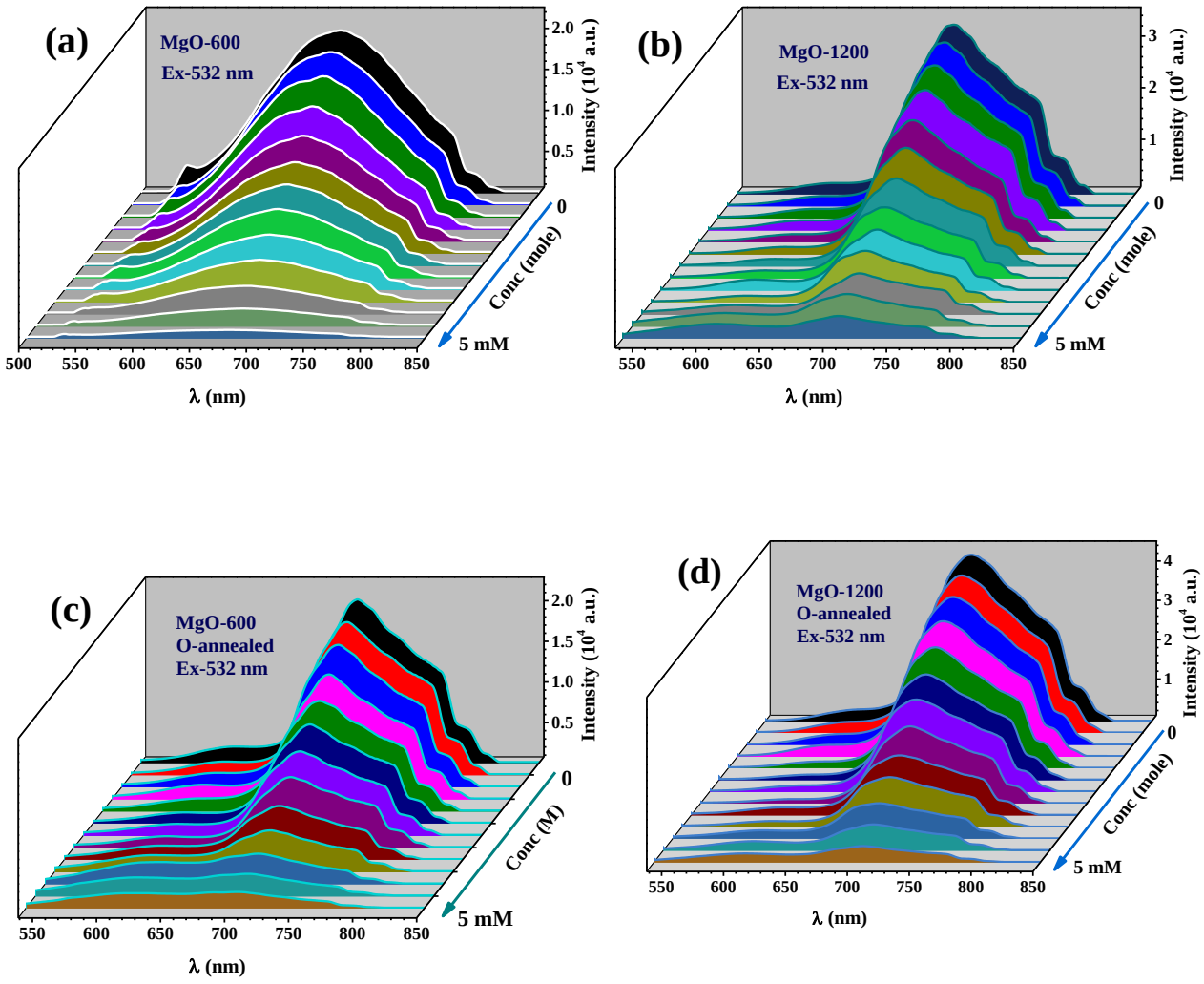

Figure S12. Variation of PL spectrum with increase in the PA concentration for (a) MgO-600, (b) MgO-1200, (c) MgO-600 (O) and (d) MgO-1200 (O), respectively with 532 nm excitation.

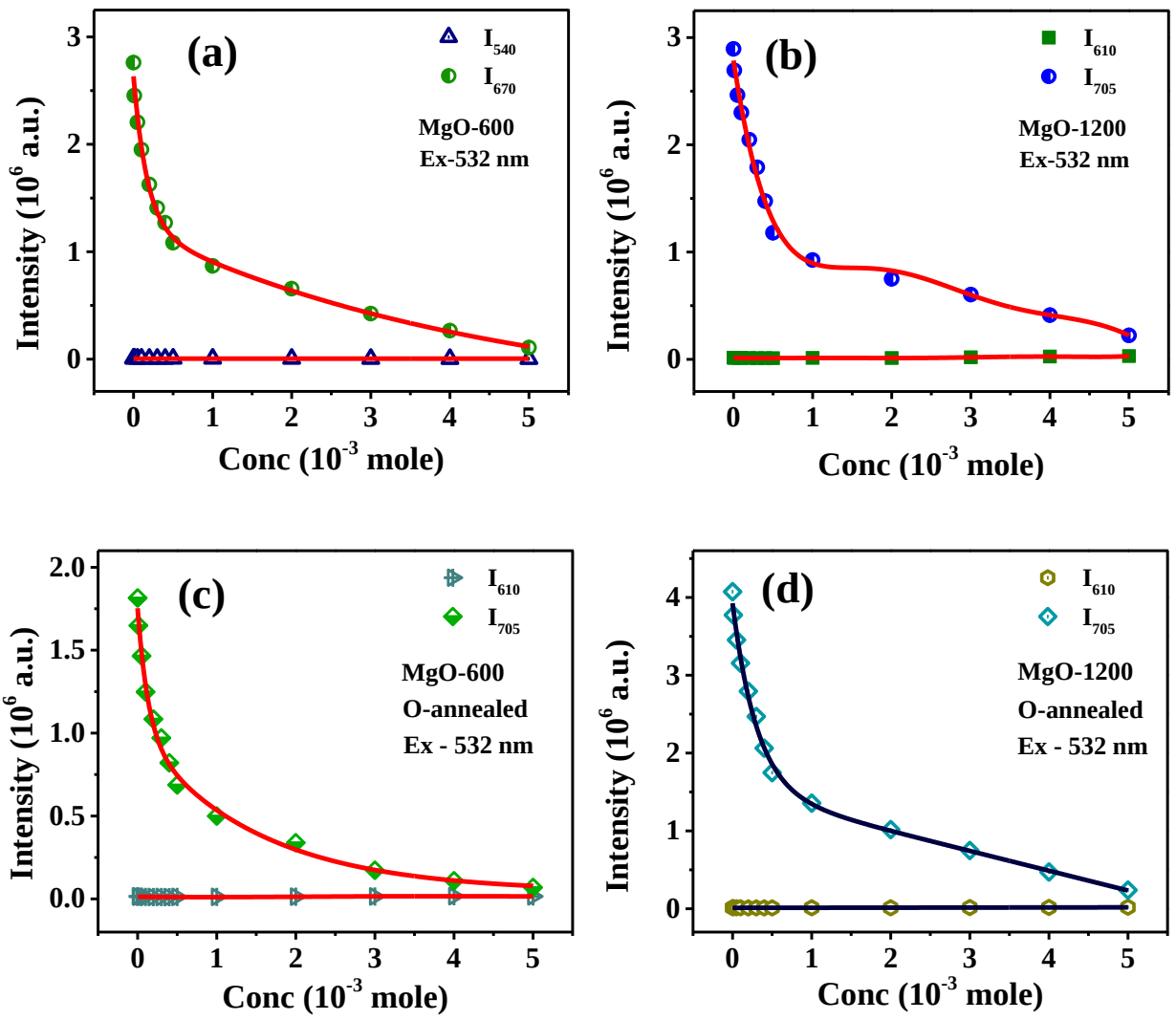

Figure S13. Variation of different integral peak intensities with increasing PA concentration of (a) MgO-600, (b) MgO-1200, (c) MgO-600 (O) and (d) MgO-1200 (O), respectively with 532 nm excitation.

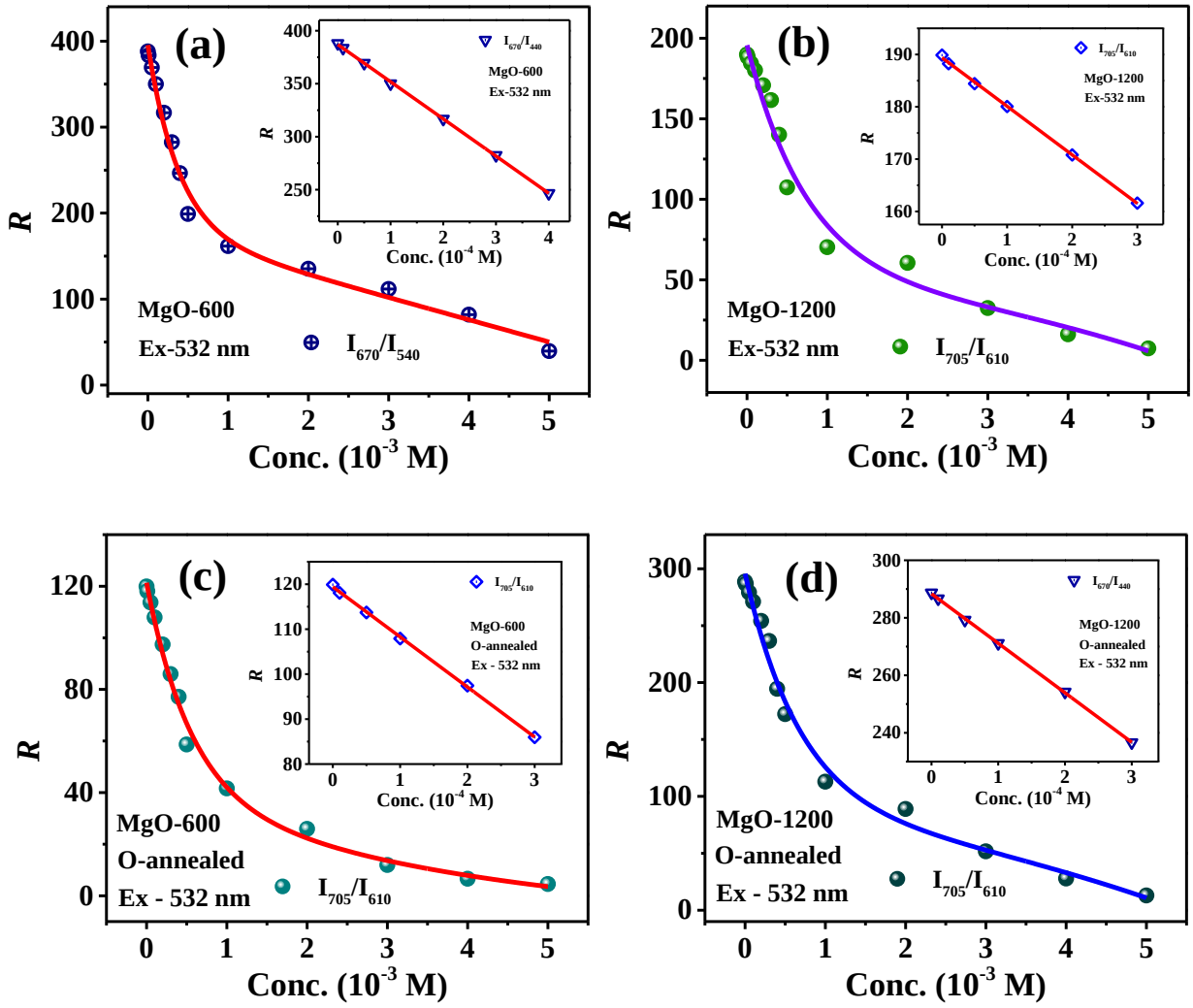

Figure S14. Variation of integral peak intensity ratio (R) with increasing PA concentration of (a) MgO-600, (b) MgO-1200, (c) MgO-600 (O) and (d) MgO-1200 (O), respectively with 532 nm excitation. Insets show corresponding linear fitting in the low PA concentration region.

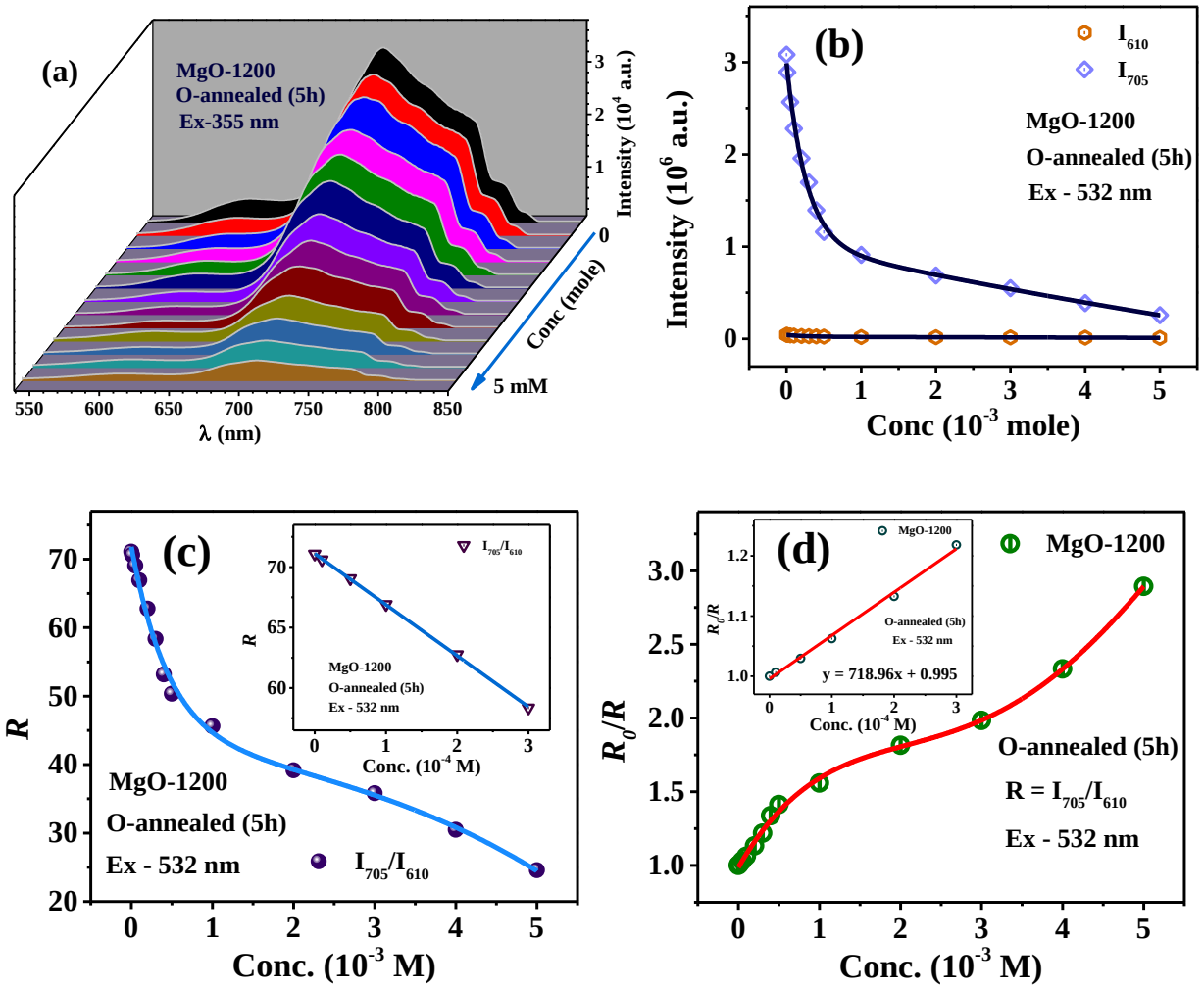

Figure S15. (a) Variation of PL spectrum with increase in the PA concentration for MgO-1200 (O-5h) with 532 nm excitation, corresponding variation of (b) different integral peak intensities and (c) integral intensity ratio with increasing PA concentration. (d) S-V plot for intensity ratio variation with PA concentration of MgO-1200 (O-5h) for 532 nm excitation. Inset of the figure (c) and (d) shows the linear fitting of the corresponding plots for low PA concentration region.

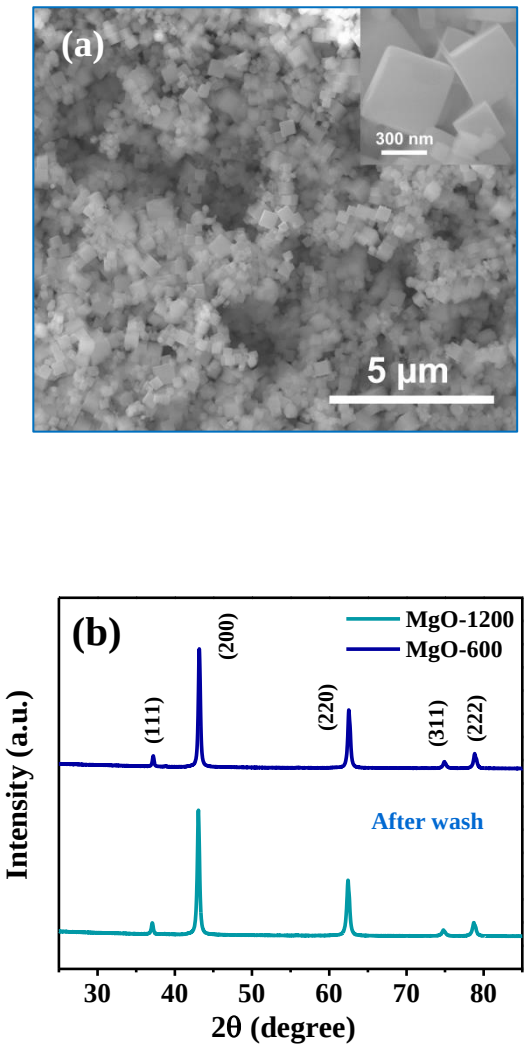

Figure S16. (a) SEM image of the washed MgO-1200 after used in cycle test for five times and (b) XRD patterns of the washed MgO-600 and MgO-1200 after cycle test (5-times with PA).

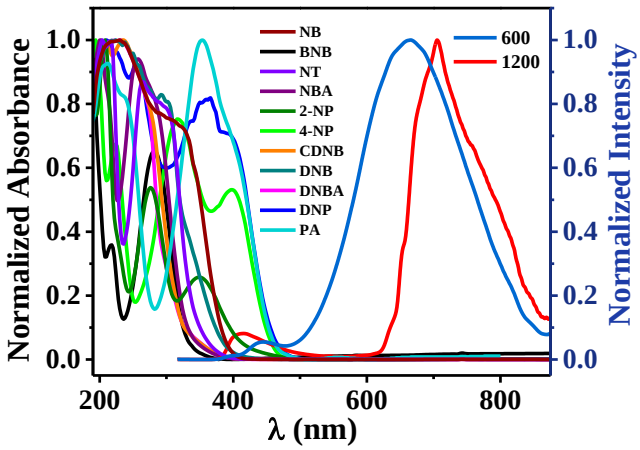

Figure S17. Spectral overlap between the absorption spectra of various nitro compounds and the emission spectra of the MgO nanocubes (MgO-600 and MgO-1200) with 355 nm excitation.

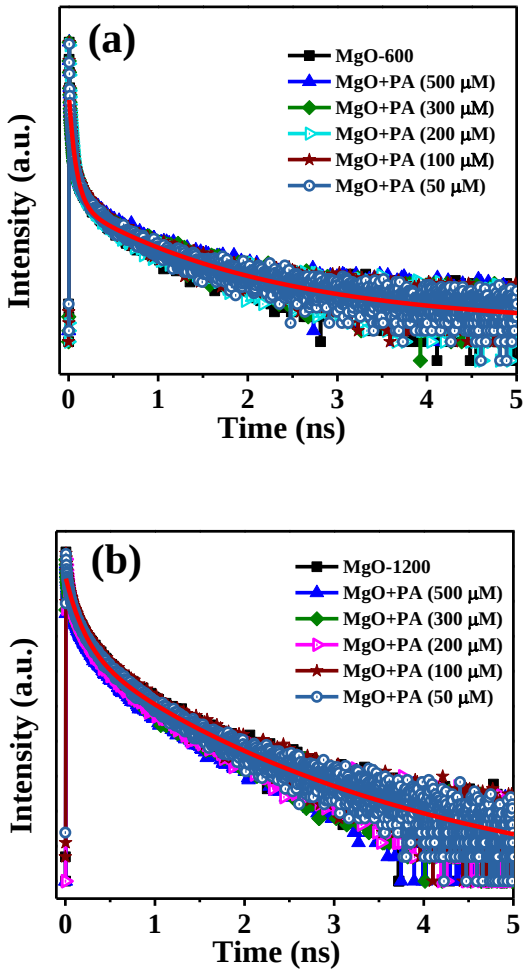

Figure S18. Time resolve PL measurement of the two samples (MgO-600 and MgO-1200) in the absence and presence of PA with 355 nm excitation and 670 and 705 nm as emission wavelength respectively for (a) MgO-600 and (b) MgO-1200.

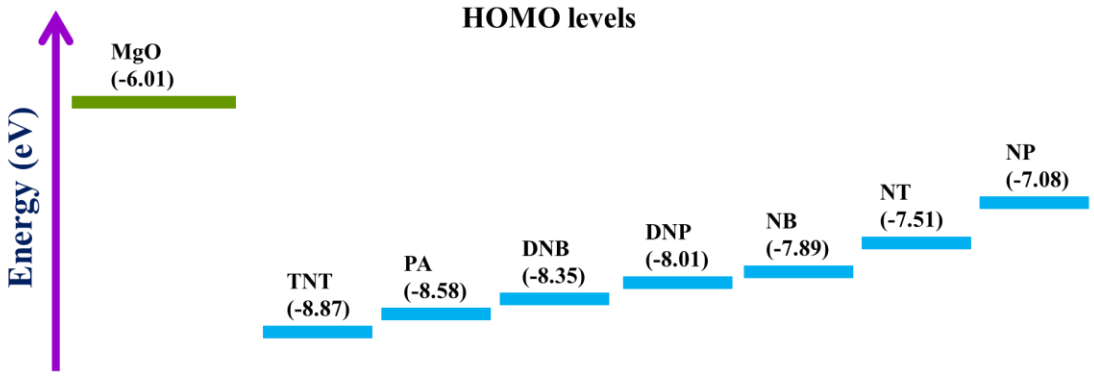

Figure S19. Pictorial representation of HOMO energy levels of MgO along with different nitro compounds.[1,2]

Table S1. Comparison table for quenching constant (K_Q) and limit of detection (*LOD*) for different MgO samples with two excitations.

Material	**Excitation (nm)**	K_Q **(M^{-1})**	***LOD*** **(10^{-6} M)**
MgO-600	355	1.1×10^3	4.74
	532	1.39×10^3	4.8
MgO-1200	355	1.6×10^3	7.55
	532	5.73×10^2	5.98
MgO-600 (O)	355	1.4×10^3	5.13
	532	1.37×10^3	5.71
MgO-1200 (O)	355	1.41×10^3	4.88
	532	7.23×10^2	3.53
MgO-1200 (O-5h)	532	7.19×10^2	3.25

Table S2. Comparison table for response time for the interaction of different concentration of PA with MgO-600 and MgO-1200 for 355 nm excitation.

PA Conc.	**Response time (sec)**	
	MgO-600	**MgO-1200**
0	0	0
100 µM	2.12	1.08
200 µM	1.57	1.07
300 µM	1.56	2.13
500 µM	2.15	1.07
1 mM	2.13	1.54
3 mM	2.39	2.13
5 mM	1.59	1.07

Table-S3. Comparison of LOD values of MgO nanocubes for PA with different reported sensor materials.

Sl. no.	Sensor materials	Sensing medium	S-V constant (M^{-1})	Detection limit (LOD)	References
1	Polyimide covalent organic nanosheets (PICONs)	Ethanol	1×10^{7}	0.25 µM	2
2	Phosphole oxide	Water/THF	2.03×10^{4}	2.03 mM	3
3	Cationic bispyrene fluorophore, Py-diIMPy	Water	----	1×10^{-6} M	4
4	Isobenzotriazolophanes	Cyclohexane	8.2×10^{2}	8.4×10^{-5} M	5
5	Mesoporous SBA-15	Water	1.4×10^{5}	2.5×10^{-5} M	6
6	Tripyrenyl truxene	Water/THF	3.6×10^{4}	0.15 ppm	7
7	Poly(acrylate) derivative	Water/THF	4.27×10^{4}	2.5 ppm	8
8	2-Amino-7-chloro-1,8-naphthyridine	Water/methanol	3.9×10^{4}	4.16 µM	9
9	MgO nanocubes	Solid state	1.6×10^{3}	3.25×10^{-6} M	Present work

Table S4. Comparison table for excited state life time in the presence and absence of different concentration of PA for MgO-600 and MgO-1200.

PA Conc. (μM)	Life time (ns)	
	MgO-600	**MgO-1200**
0	1.162	2.829
500	1.172	2.867
300	1.168	2.883
200	1.164	2.798
100	1.171	2.835
50	1.175	2.756

References:

(1) Xing, S.; Bing, Q.; Qi, H.; Liu, J.; Bai, T.; Li, G.; Shi, Z.; Feng, S.; Xu, R. Rational Design and Functionalization of a Zinc Metal−Organic Framework for Highly Selective Detection of 2,4,6-Trinitrophenol. *ACS Appl. Mater. Interfaces*, **2017**, *9*, 23828–23835, DOI: 10.1021/acsami.7b06482.

(2) Zhang, C.; Zhang, S.; Yan, Y.; Xia, F.; Huang, A.; Xian, Y. Highly Fluorescent Polyimide Covalent Organic Nanosheets as Sensing Probes for the Detection of 2,4,6-Trinitrophenol. *ACS Appl. Mater. Interfaces*, **2017**, *9*, 13415–13421, DOI: 10.1021/acsami.6b16423.

(3) Shiraishi, K.; Sanji, T.; Tanaka, M. Trace Detection of Explosive Particulates with a Phosphole Oxide. *ACS Appl. Mater. Interfaces* **2009**, *1*, 1379−1382, DOI: 10.1021/am900313g.

(4) Ding, L.; Bai, Y.; Cao, Y.; Ren, G.; Blanchard, G. J.; Fang, Y. Micelle-Induced Versatile Sensing Behavior of Bispyrene-Based Fluorescent Molecular Sensor for Picric Acid and PYX Explosives. *Langmuir* **2014**, *30*, 7645−7653, DOI: 10.1021/la5011264.

(5) Venkatesan, N.; Singh, V.; Rajakumar, P.; Mishra, A. K. Isobenzotriazolophanes: A New Class of Fluorescent Cyclophanes as Sensors for Aromatic Nitro Explosives−Picric Acid. *RSC Adv*. **2014**, *4*, 53484−53489, DOI:10.1039/C4RA06320A.

(6) Li, D.; Liu, J.; Kwok, R. T. K.; Liang, Z.; Tang, B. Z.; and Yu, J. Supersensitive detection of explosives by recyclable AIE luminogen-functionalized mesoporous materials. *Chem. Commun*. **2012**, *48*, 7167–7169, DOI:10.1039/C2CC31890C.

(7) Samang, P.; Raksasorn, D.; Sukwattanasinitt, O.; Rashatasakhon, P. A Nitroaromatic Fluorescence Sensor from a Novel Tripyrenyl Truxene. *RSC Adv*. **2014**, *4*, 58077−58082, DOI:10.1039/C4RA11407H.

(8) Zhou, H.; Li, J.; Chua, M. H.; Yan, H.; Tang, B. Z.; Xu, J. Poly(acrylate) with a Tetraphenylethene Pendant with Aggregation-induced Emission (AIE) Characteristics: Highly Stable AIE-active Polymer Nanoparticles for Effective Detection of Nitro Compounds. *Polym. Chem.* **2014**, *5*, 5628–5637, DOI:10.1039/C4PY00518J.

(9) Chahal, M. K.; Sankar, M. 1,8-Naphthyridine-based fluorescent receptors for picric acid detection in aqueous media. *Anal. Methods* **2015**, *7*, 10272–10279, DOI:10.1039/C5AY01464F.